# Evidence for an Induced-Fit Mechanism Operating in Pi Class Glutathione Transferases[†,‡]

Aaron J. Oakley,[§] Mario Lo Bello,[||] Giorgio Ricci,[||] Giorgio Federici,[⊥] and Michael W. Parker*[,§]

*The Ian Potter Foundation Protein Crystallography Laboratory, St. Vincent's Institute of Medical Research, 41 Victoria Parade, Fitzroy, Victoria 3065, Australia, Department of Biology, University of Rome "Tor Vergata", Via della Ricerca Scientifica, 00133 Rome, Italy, and Ospedale Pediatrico IRCCS "Bambin Gesù", 00165 Rome, Italy*

*Received February 9, 1998; Revised Manuscript Received March 24, 1998*

ABSTRACT: Three-dimensional structures of the apo form of human pi class glutathione transferase have been determined by X-ray crystallography. The structures suggest the enzyme recognizes its substrate, glutathione, by an induced-fit mechanism. Compared to complexed forms of the enzyme, the environment around the catalytic residue, Tyr 7, remains unchanged in the apoenzyme. This observation supports the view that Tyr 7 does not act as a general base in the reaction mechanism. The observed cooperativity of the dimeric enzyme may be due to the movements of a helix that forms one wall of the active site and, in particular, to movements of a tyrosine residue that is located in the subunit interface.

Glutathione S-transferases (GSTs,[1] EC 2.5.1.18) are multifunctional enzymes involved in the detoxification of endogenous and foreign toxins. The most important reaction catalyzed by GSTs is the addition of glutathione (γ-glutamylcysteinylglycine, GSH) to hydrophobic molecules with electrophilic centers. Mammalian cytosolic GSTs can be divided into seven classes: alpha, mu, pi, theta, sigma, kappa, and zeta on the basis of sequence similarity, substrate specificity, and three-dimensional structure (*1*−*5*). All of the cytosolic isozymes are homo- or heterodimers; however no interclass heterodimers have so far been observed (*6*). The human pi class GST (hGST P1-1) is the most widely distributed and the most abundant isozyme. GSTs have been observed in both in vitro and in vivo studies to be overexpressed in a diverse range of neoplastic cells (for a review, see ref *7*). These and other studies have implicated the enzyme in the development and resistance of tumors toward commonly used anticancer drugs. Understanding the structure and kinetics of the human P1-1 isoenzyme is therefore of great interest (for recent reviews, see refs *6*, *7*).

A number of pi class GST crystal structures have been determined in recent years leading to an improved understanding of how the enzyme recognizes and reacts with a broad range of substrates (*8*−*16*). Each monomer consists of two domains and possesses one active site. The GSH binding site is made up of residues mostly from the N-terminal domain (Figure 1), while the binding site for electrophilic substrates is made up of residues from both domains. Studies on the kinetics of hGST P1-1 have revealed the importance of structural flexibility to the function of the enzyme (*17*−*18*). The crystal structures suggest that helix α2 and its flanking regions (residues 35−51) are a prime candidate for the flexible regions that influence catalysis. This region forms one wall of the GSH binding site and contributes a number of ligands (Trp 38, Lys 44, and Gln 51) to GSH binding (Figure 1). Nevertheless, it is a highly flexible portion of the molecule as judged by crystallographic temperature factors (*9*, *14*). There is biochemical evidence suggesting that this region is highly flexible in the absence of GSH and is critical for activity. The apoenzyme loses all activity when treated with trypsin, which cleaves the peptide bond between Lys 44 and Ala 45, whereas the presence of GSH protects the enzyme against proteolysis (*19*). Fluorescence experiments suggest that an increase of about 4 Å in the distance between helix α2 and helix α4 occurs upon binding of GSH (*18*). Chemical modification of a reactive cysteine residue, Cys 47, causes inactivation of the enzyme (*20*). This residue is not located in the active site but nearby, on the C-terminal end of helix α2 where it is buried within a surface hydrophobic pocket. Flexibility of helix α2 is required for this cysteine to become accessible. Chemical modification would cause a shift in the helix, disturbing the position of some essential GSH ligands and hence causing inactivation. Mutation of all cysteine residues in hGST P1-1 to serine has shown that they are not essential for catalytic activity (*21*); however oxidation results in the formation of an intramonomer disulfide bond between Cys 47 and Cys 101, with subsequent inactivation of the enzyme (*22*, *23*). This is remarkable because the sulfur atoms of these residues are separated by 18.4 Å in the crystal structure (*9*), indicating that helix α2 must be highly flexible.

[†] Financial support from the Australian Research Council and the National Research Council of Italy is gratefully acknowledged. A.J.O. was a recipient of a National Health & Medical Research Council Postgraduate Research Scholarship and an International Centre for Diffraction Data Crystallography Scholarship, and M.W.P. is an Australian Research Council Senior Research Fellow.

[‡] The crystallographic coordinates have been deposited in the Brookhaven Protein Data Bank under the filenames 14GS and 16GS.

* Corresponding author. Tel: +61 3 9288 2480. Fax: +61 3 9416 2676. E-mail: mwp@rubens.its.unimelb.edu.au.

[§] St. Vincent's Institute of Medical Research.

[||] University of Rome "Tor Vergata".

[⊥] Osp. Pediatrics IRCCS "Bambin Gesù".

[1] Abbreviations: DTT, 1,4-dithiothreitol; EDTA, ethylenediamine tetraacetic acid; GSH, glutathione; GST, glutathione S-transferase; MES, 2-[*N*-morpholino]ethanesulfonic acid; NCS, noncrystallographic symmetry.

S0006-2960(98)00323-7 CCC: $15.00 
Published on Web 06/23/1998

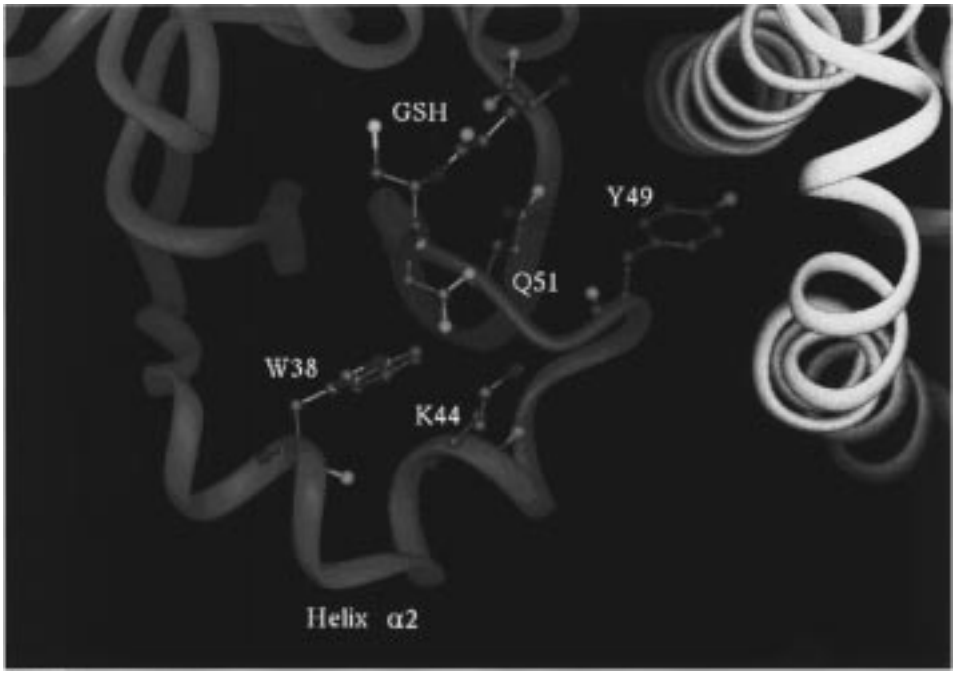


FIGURE 1: A ribbon picture of the GSH binding domain of hGST P1-1 (14). The GSH molecule is shown in ball-and-stick. Helix α2 is denoted, and residues from this helix and its flanking regions that directly contact GSH are also shown in ball-and-stick. Tyr 49, a residue implicated in the cooperativity of the enzyme, is also shown in ball-and-stick. This figure was produced by the computer program INSIGHT II (Molecular Simulations Inc., San Diego, CA).

Further investigation revealed that the mutation Cys 47 to Ser or Ala reduces GSH affinity in the apoenzyme and induces positive cooperativity for GSH (*24*). The molecular basis for the structural communication between the subunits is not known.

There are now numerous reported structures of the pi class GST from human, pig, and mouse in complex with a variety of substrates and inhibitors (*8*−*16*). However, there has been no report of an apo structure because of difficulties met in crystallizing this form of the enzyme. Since the biochemical evidence suggests that helix α2 plays a vital role in the catalytic mechanism of hGST P1-1, the structure of the apoenzyme is of great importance toward understanding the mechanism of catalysis in the enzyme. Here we report two different structures of the apoenzyme, called Apo1 and Apo2. These structures show that the substrate, GSH, is recognized by an induced-fit mechanism, supports the view that a key tyrosine residue does not play a role as a general base in the catalytic mechanism, and provides structural insights into understanding the observed cooperativity of the enzyme.

## EXPERIMENTAL PROCEDURES

*Crystallization and Data Collection.* All crystals were grown using the hanging drop technique (*25*). For Apo1, a 2 μL droplet of an 8 mg/mL protein solution containing 10 mM phosphate buffer (pH 7.0), 1 mM EDTA, and 2 mM β-mercaptoethanol was mixed with 2 μL of 1 mM adriamycin−GSH solution (where the solution was made by dissolving solid powder in distilled water) and allowed to stand for up to 30 min before adding 2 μL of reservoir solution. The adriamycin−GSH sample was a gift from Dr. Giorgio Gaudiano (Istituto di Medicina Sperimentale, CNR, Rome, Italy). The reservoir solution consisted of 28% (w/v) ammonium sulfate, 65−75 mM DTT, 100 mM MES buffer (pH range 6.4−6.8), and 5% (v/v) dimethyl sulfoxide. The trials were carried out at a constant temperature of 22 °C. The drops were allowed to equilibrate for 2 days before they were streak-seeded with a cat's whisker from drops containing crystals grown under similar conditions. Maroon-colored crystals appeared in the shape of plates after one week and grew to maximal dimensions of 0.1 mm × 0.4 mm × 0.4 mm. For Apo2, a 2 μL droplet of a 12 mg/mL protein solution containing 10 mM phosphate buffer (pH 7.0), 1 mM EDTA, and 2 mM β-mercaptoethanol was mixed with 2 μL of reservoir solution. This protein had been passed over a G-25 column in an attempt to remove the GSH. The reservoir solution consisted of 23% (w/v) ammonium sulfate, 55 mM DTT, and 100 mM MES buffer (pH 5.8). The drops were allowed to equilibrate for 2 days at 22 °C before they were streak-seeded with a cat's whisker from drops containing crystals grown under similar conditions. After the crystals were fully grown, the anticancer drug, chlorambucil (obtained from Sigma Chemical Co, St. Louis, MO), was added as a powder to the drop. The crystals were then left for 24 days before data collection.

All X-ray diffraction data were collected on a MAR-Research area detector with Cu Kα X-rays generated by a Rigaku RU-200 rotating anode X-ray generator. An Oxford Cryosystems Cryostream Cooler was used to maintain Apo2 crystals at low temperature, whereas the Apo1 data were collected from crystals at room temperature. The diffraction data were processed and analyzed using programs in the HKL (*26*) and CCP4 (*27*) suites. The statistics showing the quality of the X-ray data are presented in Table 1.

*Structure Solution and Refinement.* The initial analysis of the data included examination of difference Fourier maps calculated with $\sigma_A$-weighted $F_o - F_c$ and $2F_o - F_c$ coefficients (*28*) where native amplitudes and phases were calculated from the final 2.0 Å resolution model of hGST P1-1 complexed with GSH (*14*) after ligands and solvent

Table 1: Data Collection and Refinement Statistics[a]

| | Apo1 | Apo2 |
|---|---|---|
| **Data Collection Statistics** | | |
| space group | *C2* | *C2* |
| data collection temperature (K) | 288 | 100 |
| cell dimensions | | |
| *a* (Å) | 78.7 | 77.5 |
| *b* (Å) | 91.8 | 89.8 |
| *c* (Å) | 69.1 | 68.7 |
| $\beta$ (deg) | 98.3 | 97.8 |
| maximum resolution (Å) | 2.8 | 1.9 |
| total no. of observations | 17 349 | 96 823 |
| no. of unique reflections | 10 691 | 34 323 |
| completeness of data (%) | 88.6 (91.3) | 95.1 (91.5) |
| completeness of data $>3\sigma_I$ (%) | 57.8 (17.0) | 72.4 (33.1) |
| $I/\sigma_I$ | 6.6 (1.5) | 17.7 (2.6) |
| multiplicity | 1.6 | 2.8 |
| $R_{merge}$ (%)[b] | 7.5 (40.7) | 5.3 (32.9) |
| **Refinement Statistics** | | |
| non-hydrogen atoms | | |
| protein | 3054 | 3262 |
| buffer | 24 | 24 |
| sulfate | 0 | 5 |
| solvent | 5 | 298 |
| resolution (Å) | 2.8 | 1.9 |
| $R_{factor}$ (%)[c] | 19.0 (29.5) | 22.7 (36.6) |
| $R_{free}$ (%) | 24.0 (35.5) | 26.3 (36.0) |
| reflections used in $R_{factor}$ calculations | | |
| number | 10 236 | 32 594 |
| completeness (%) | 80.6 | 88.5 |
| rmsd's from ideal geometry | | |
| bonds (Å) | 0.007 | 0.007 |
| angles (deg) | 1.27 | 1.28 |
| dihedrals (deg) | 22.20 | 23.17 |
| impropers (deg) | 1.29 | 0.82 |
| bonded *B*'s (Å$^2$) | 4.95 | 2.94 |
| residues in most favored regions of ramachandran plot (%) | 91.5 | 94.1 |

[a] The values in parentheses are for the highest-resolution bin (approximate interval of 0.1 Å). [b] $R_{merge} = \sum_{hkl} \sum_i |I_i - \langle I \rangle| / |\langle I \rangle|$, where $I_i$ is the intensity for the *i*th measurement of an equivalent reflection with indices *h*, *k*, and *l*. [c] $R_{factor} = \sum_{hkl} ||F_{obs}| - |F_{calc}|| / \sum |F_{obs}|$, $R_{free}$ was calculating using 5% of the data.

molecules were removed. The $2F_o - F_c$ electron density maps were further improved by 10 cycles of 2-fold non-crystallographic symmetry (NCS) averaging using the RAVE package (*29*). If there was uncertainty in the correct interpretation of density, omit maps were created by deleting the relevant region of the protein, subjecting it to positional refinement, and generating maps from the resulting model. X-PLOR (30) was used for the refinement of all structures. The initial models were subjected to rigid body refinement before being subjected to NCS-restrained positional and temperature factor refinement. Subsequent cycles of refinement consisted of model rebuilding with O (*31*) followed by positional and temperature factor refinement. The temperature factors were refined in all cases with NCS restraints, and the weights were chosen on the basis of the behavior of $R_{free}$ and sensible temperature factor trends. In the early cycles of refinement, all reflections between 8.0 Å and the high-resolution limit were used. In the final cycles, all reflections were used for refinement, in conjunction with a bulk solvent correction.

The starting model for Apo1 had an $R_{factor}$ of 41.7% ($R_{free}$ = 34.2%). Maps generated from this model after rigid body refinement revealed no density in the H-site or the G-site or for residues 36−48 inclusive. The missing residues were omitted from the model. Otherwise, the density for the rest of the protein was of good quality. Density was visible for two MES molecules, which stacked against residue Trp 28 in each monomer. These were built into density. After 4 rounds of positional and B-factor refinement, the $R_{factor}$ was 21.5% ($R_{free}$ = 27.4%). At this stage, a bulk solvent correction was applied. After two more rounds of positional and temperature factor refinement, the $R_{factor}$ was 19.0% ($R_{free}$ = 24.0%). At no time was electron density observed for any part of the adriamycin−GSH molecule. $2F_{obs} - F_{calc}$ electron density maps calculated at very low contour levels ($<0.5\sigma$) indicate the complete absence of GSH in the G-site.

The starting model for Apo2 ($R_{factor}$ = 37.2%, $R_{free}$ = 37.2%) was subjected to rigid body refinement to give a model with $R_{factor}$ = 34.2% ($R_{free}$ = 33.7%). Two rounds of refinement were performed during which water molecules, two MES molecules, and a sulfate ion were built into the structure. Good density for the entire protein was observed with the exception of the region about helix α2 and its flanking regions which was poor. However, the density for this region was interpretable and hence was included in the model. After two rounds of refinement, with a bulk solvent correction, the final model had an $R_{factor}$ of 22.7% ($R_{free}$ = 26.3%). At no time was electron density observed for any part of the chlorambucil molecule. $2F_{obs} - F_{calc}$ electron density maps calculated at very low contour levels ($<0.5\sigma$) indicated a few small spheres of electron density compatible with the presence of water molecules in the G-site but showed no evidence of any bound GSH.

The final refinement statistics of all models are presented in Table 1. Stereochemical analysis with PROCHECK (*32*) demonstrated the high stereochemical quality of the refined structures. The coordinates have been deposited in the Broohaven Protein Data Bank with accession numbers 14GS (Apo1) and 16GS (Apo2).

## RESULTS

Our initial attempts to crystallize the apoenzyme were frustrated by the fact that the enzyme is purified by elution with GSH from affinity columns, and attempts to remove GSH from the enzyme proved difficult. Here we present two apoenzyme structures which we call Apo1 and Apo2 (Table 1). The structures were derived from GSH-bound crystals that were soaked in the presence of inhibitors. In Apo1, the crystals had been grown in the presence of adriamycin−GSH, the GSH conjugate of the anticancer drug. However, no density was observed in the active site, with the exception of density for water molecules, at any stage during the refinement. In hindsight, we suspect the carrier solvent, dimethyl sulfoxide, used in the crystallization trials was responsible for the production of the apoenzyme. We hypothesize that adriamycin−GSH displaced the GSH that was bound to the enzyme, and then, upon addition of the organic solvent, the GSH conjugate was removed from the active site. In Apo2, the crystals were soaked in the anticancer drug, chlorambucil. Again there was no evidence of any ligand in the active site. In this case the treatment of the protein on the G-25 column may have successfully produced the apoenzyme, and the crystallization conditions did not favor binding of the poorly water soluble chloram-

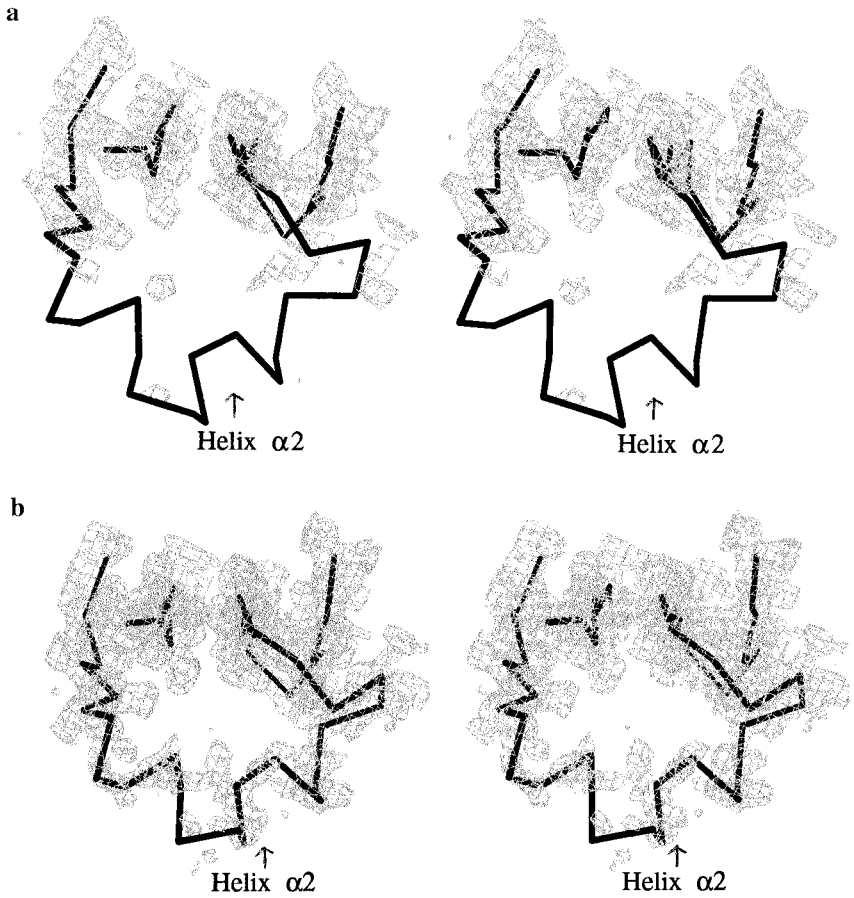


FIGURE 2: Stereo diagrams of the final $2F_{obs} - F_{calc}$ electron density maps of the apoenzyme structures showing the GSH binding domain of hGST P1-1. The maps were calculated using all reflections (see Table 1) and contoured at the 1.0$\sigma$ level. The view is the same as shown in Figure 1. The electron density is indicated in light gray shading, and the alpha carbon backbone of the enzyme, as observed in the GSH complex (*14*), is shown in thickened lines. Helix α2, indicated by the arrow, is strictly made up of two helices (residues 35−40 and 42−44) with a break at residue Gly 41; (a) Apo1; (b) Apo2.

bucil molecule. Both structures have been crystallized in the *C2* space group where there are no crystal contacts involving helix α2 and its flanking regions in either monomer (*14*).

Portions of the electron density maps in the vicinity of the active site of hGST P1-1 are shown in Figure 2. Surprisingly, the two apo structures show significant differences. In Apo1, the region spanning residues 36−48 has no convincing density in either monomer (Figure 2a). In the case of Apo2, good quality electron density was observed for all of the enzyme, except for helix α2 (residues 35−44) and its flanking regions where the density was poor (Figure 2b). However, omit maps of this region showed sufficient density to be able to include the helix in the model. No density was seen for residues 39−41, and only poor density was observed for residues 35−39 and 41−47. Good density was observed for the side chain of residue Trp 38 and for residues Leu 48 and Tyr 49. The observation of poor or no visible electron density in regions of both structures is indicative of either high mobility or multiple conformational states of those regions. We suspect that one of the reasons for the differences in the structures of Apo1 and Apo2 is the temperature of data collection and the use of glycerol as a cryoprotectant. Apo1 was measured at room temperature, whereas Apo2 was measured at 100 K. Glycerol has been used previously as a viscosogen in studying the effect of viscosity on kinetics of the enzyme (*18*). The results showed that the affinity for GSH increased with increasing glycerol concentration. The low temperature of data collection and the use of glycerol in the Apo2 crystal experiments may explain the better density for helix α2 compared to that of Apo1. Because helix α2 is well-defined in the complexed form of the enzyme, determined at the same resolution and temperature as Apo1 (*9*), the binding of GSH must lock this region into place.

Another intriguing difference between the structures is a movement of the side chain of residue Tyr 49. In the structure of the complexed enzyme, the hydroxyl group of this residue is in hydrogen bonding distance (2.8 Å) of the main chain carbonyl oxygen of Met 91 from the opposing monomer. Whereas in Apo2, the distance is the same within experimental error, this is not the case for Apo1 where the distance is 4.3 Å (Figure 3). This represents a 2.4 Å movement of the hydroxyl group away from its position in the complexed enzyme. (In Apo2 the hydroxyl group moves by 0.7 Å, but this is close to the estimated coordinate error. It is however tempting to suggest that Tyr 49 has moved in this structure correlating with the increased flexibility of the helix α2 region.) In the GSH complex, Tyr 49 is involved in 15 van der Waals and hydrogen bonding contacts with the other monomer, while in Apo1 there are only 8 such contacts. As well as the loss of the hydrogen bonding interaction, van der Waals interactions are lost with Val 92 and Pro 128 of the opposing subunit. In summary, the

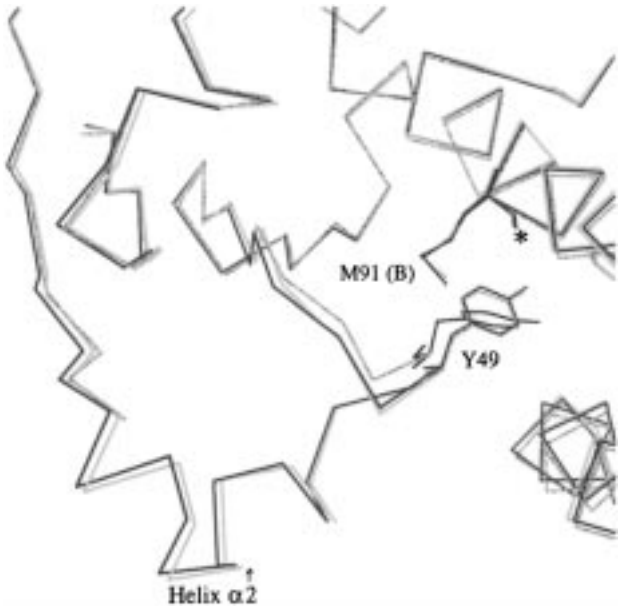


FIGURE 3: Superposition of the alpha carbon backbones of the two apoenzyme and GSH complex structures in the vicinity of Tyr 49 which is located in the dimer interface. The view is the same as shown in Figure 1. The side chains of Tyr 49 and Met 91 (from subunit B) are shown, and the carbonyl oxygen of Met 91 is indicated by an asterisk. The structures are colored as follows: gray with Tyr 49 side chain in black, Apo1; yellow, Apo2; and green, GSH complex (*14*).

disappearance of helix α2 in the electron density maps appears to be associated with movement of Tyr 49 and the loss of some intersubunit contacts.

Besides the movement of the tyrosine side chain and the differences in the helix α2 region, the apo structures superimpose closely with the previously determined GSH complex (*14*). The rms differences in the position of Cα atoms between the structures of the dimers are 0.44 and 0.17 Å for the Apo1 and Apo2 structures, respectively. In the higher-resolution Apo2 structure, water molecules are located in the position where GSH would bind and a chain of three water molecules link Tyr 7 to Tyr 108 (another catalytic residue). The temperature factor trends (data not shown) for all structures are similar, with the exception of helix α2 and the helical towers in the dimer interface which show varying temperature factors. The structures can be placed in order of decreasing temperature factors for helix α2 as follows: Apo1 > Apo2 > GSH complex (*14*). The temperature factors for the C-terminal end of helix α4, the following coil, and the N-terminal region of helix α5 follow a trend similar to those for helix α2.

## DISCUSSION

It has long been accepted that ligands may stabilize native structures of proteins. The evidence presented here suggests that helix α2 of hGST P1-1 can become highly mobile in the absence of GSH and is stabilized by substrate binding. Helix α2 contains residues involved in binding the substrate GSH, and the stabilization of this region upon GSH binding may result in a lower free energy for the structure, thus contributing to the enzyme's affinity for this ligand. The greatly increased flexibility of helix α2 observed in the crystal structures presented here provides an explanation of how a disulfide bond can form between Cys 47, which resides on this helix, and Cys 101 in the oxidized form of the free enzyme (*22*, *23*). These residues are more than 18 Å apart in the complexed and Apo2 structures, and mobility of helix 2 as seen here is required for them to get close enough for disulfide bond formation.

The microenvironment around the catalytic residue, Tyr 7, appears identical in both apo and complexed structures (*14*) of the enzyme. In the apo structures, Tyr 7 is in hydrogen bonding distance of the Nϵ atom of Arg 13 and of a water molecule which occupies the position where the sulfur atom sits in the GSH complex. These observations suggest that Tyr 7 is protonated in the apoenzyme. The absence of a nearby positively charged group in the apo structures and the lack of movement of the side chain between apo and the GSH complex support the proposal that Tyr 7 does not become ionized in the reaction mechanism (*6*). Thus Tyr 7 does not appear to play a role as a general base to abstract a proton from the thiol group of the substrate, GSH.

The alpha, mu, and pi class GSTs contain an aromatic residue (Tyr 49 in the hGST P1-1) in the loop between helix α2 and sheet β3 which contacts the opposing monomer. This residue acts as a hydrophobic lock in subunit dimerization (*6*). Tyr 49 has less van der Waals contacts with the adjacent monomer in the Apo1 structure than it does in the GSH bound form of the enzyme (Figure 3). The reduced contacts could, in part, account for the elevated temperature factors observed for the regions spanning helices α4 and α5 which line the interface. The change in Tyr 49 contacts could be one way in which the two active sites of the GST dimer could affect each other. The observed cooperativity resulting from mutation of Cys 47 (*24*) could be explained by increased flexibility of the region around helix α2 and with the resulting effects being transmitted through residue Tyr 49 to the opposing monomer.

The different apoenzyme structures presented here, in conjunction with the structure of the GSH complex of the enzyme (*14*), allow us to make some observations about the changes that occur to the enzyme in the transition from apoenzyme to GSH-bound form. First, helix α2, which is essential for the binding of this substrate, is disordered in the absence of the substrate. The nature of the disorder (static versus dynamic versus a number of discrete conformational states) cannot be determined from the data presented here. However, the observation of density for the helix in the apo structure at low temperature suggests that the helix may stay relatively intact at physiological temperatures. The results suggest that binding of GSH is accompanied by closer association and stabilization of the monomers as shown by a decrease in the temperature factors of the helical towers and by a decreasing Tyr 49 hydroxyl to Met 91 carbonyl oxygen distance. These changes may account for the kinetics observed for the cooperative mutants.

There have been reports of three apoenzyme structures from other GST classes: human alpha class GST (*33*), a mu class GST from *Schistosoma japonica* (*34*), and a theta class GST from maize (*35*). In the first two cases no significant changes were observed in the helix α2 region. In the maize apoenzyme, this region exhibited poor electron density and high mobility whereas in the complexed enzyme this region appeared well-ordered (*35*, *36*). These results mirror those of the human pi enzyme reported here. All together, these observations suggest that the helix α2 region performs

a class-specific role. In the pi and plant theta class enzymes it acts by modulating the affinity of the active site for substrate.

## REFERENCES


1. Mannervik, B., Ålin, P., Guthenberg, C., Jensson, H., Tahir, M. K., Warholm, M., and Jornvall, H. (1985) *Proc. Natl. Acad. U.S.A. 82*, 7202−7206.
2. Meyer, D. J., Coles, B., Pemble, S. E., Gilmore, K. S., Fraser, G. M., and Ketterer, B. (1991) *Biochem. J. 274*, 409−414.
3. Buetler, T. M., and Eaton, D. L. (1992) *Environ. Carcinog. Ecotoxicol. Rev. C10*, 181−203.
4. Pemble, S. E., Wardle, A. F., and Taylor, J. B. (1996) *Biochem. J. 319*, 749−754.
5. Board, P. G., Baker, R. T., Chelvanayagam, G., and Jermiin, L. S. (1997) *Biochem. J. 328*, 929−935.
6. Armstrong, R. N. (1997) *Chem. Res. Toxicol. 10*, 2−18.
7. Hayes, J. D., and Pulford, D. J. (1995) *Crit. Rev. Biochem. Mol. Biol. 30*, 445−600.
8. Reinemer, P., Dirr, H. W., Ladenstein, R., Schäffer, J., Gallay, O., and Huber, R. (1991) *EMBO J. 10*, 1997−2005.
9. Reinemer, P., Dirr, H. W., Ladenstein, R., Huber, R., Lo Bello, M., Federici, G., and Parker, M. W. (1992) *J. Mol. Biol. 227*, 214−226.
10. García-Sáez, I., Párraga, A., Phillips, M. F., Mantle, T. J., and Coll, M. (1994) *J. Mol. Biol. 237*, 298−314.
11. Dirr, H., Reinemer, P., and Huber, R. (1994) *J. Mol. Biol. 243*, 72−92.
12. Ji, X., Tordova, M., O'Donnell, R., Parsons, J. F., Hayden, J. B., Gilliland, G. L., and Zimniak, P. (1997) *Biochemistry 36*, 9690−9702.
13. Lo Bello, M., Oakley, A. J., Battistoni, A., Mazzetti, A. P., Nuccetelli, M., Mazzarese, G., Rossjohn, J., Parker, M. W., and Ricci, G. (1997) *Biochemistry 36*, 6207−6217.
14. Oakley, A. J., Lo Bello, M., Battistoni, A., Ricci, G., Rossjohn, J., Villar, H. O., and Parker, M. W. (1997) *J. Mol. Biol. 274*, 84−100.
15. Oakley, A. J., Rossjohn, J., Lo Bello, M., Caccuri, A. M., Federici, G., and Parker, M. W. (1997) *Biochemistry 36*, 576−585.
16. Prade, L., Huber, R., Manoharan, T. H., Fahl, W. E., and Reuter, W. (1997) *Structure 5*, 1287−1295.
17. Caccuri, A. M., Ascenzi, P., Antoninio, G., Parker, M. W., Oakley, A. J., Chiessi, E., Nuccetelli, M., Battistoni, A., Bellizia, A., and Ricci, G. (1996) *J. Biol. Chem. 271*, 16193−16198.
18. Ricci, G., Caccuri, A. M., Lo Bello, M., Rosato, N., Mei, G., Nicotra, M., Chiessi, E., Mazzetti, A. P., and Federici, G. (1996) *J. Biol. Chem. 271*, 16187−16192.
19. Lo Bello, M., Pastore, A., Petruzzelli, R., Parker, M. W., Wilce, M. C. J., Federici, G., and Ricci, G. (1993) *Biochem. Biophys. Res. Commun. 194*, 804−810.
20. Lo Bello, M., Petruzzelli, R., De Stefano, E, Tenedini, C., Barra, D., and Federici, G. (1990) *FEBS Lett. 263*, 389−391.
21. Kong, K.-H., Inoue, H., and Takahashi, K. (1991) *Biochem. Biophys. Res. Commun. 181*, 748−755.
22. Ricci, G., Del Boccio, G., Pennelli, A., Lo Bello, M., Petruzzelli, R., Caccuri, A. M., Barra, D., and Federici, G. (1991) *J. Biol. Chem. 266*, 21409−21415.
23. Shen, H., Tamai, K., Satoh, K., Hatayama, I., Tsuchida, S., and Sato, K. (1991) *Arch. Biochem. Biophys. 286*, 178−182.
24. Ricci, G., Lo Bello, M., Caccuri, A. M., Pastore, A., Nuccetelli, M., Parker, M. W., and Federici, G. (1995) *J. Biol. Chem. 270*, 1243−1248.
25. McPherson, A. (1982) *The Preparation and Analysis of Protein Crystals*, Wiley, New York.
26. Otwinowski, Z. (1993) in *Data Collection and Processing* (Sawyer, L., Isaacs, N., and Bailey, S., Eds.) pp 56−62, SERC Daresbury Laboratory, Warrington, U.K.
27. CCP4 Suite (1994) *Acta Crystallogr. D50*, 750−763.
28. Read, R. J. (1986) *Acta Crystallogr. A42*, 140−149.
29. Kleywegt, G., and Jones T. A. (1994) in *From First Map to Final Model* (Bailey, S., Hubbard, R., and Waller, D., Eds.) pp 59−66, EPSRC, Daresbury Laboratory, Warrington, U.K.
30. Brünger, A. T. (1993) *X-PLOR, Version 3.1*, Yale University Press, New Haven, Connecticut.
31. Jones, T. A., Zou, J.-Y., Cowan, S. W., and Kjeldgaard, M. (1991) *Acta Crystallogr. A47*, 110−119.
32. Laskowski, R. A., McArthur, M. W., Moss, D. S., and Thorton, J. M. (1993) *J. Appl. Crystallogr. 26*, 282−291.
33. Cameron, A. D., Sinning, I., L'Hermite, G., Olin, B., Board, P. G., Mannervik, B., and Jones, T. A. (1995) *Structure 3*, 717−727.
34. McTigue, M. A., Williams, D. R., and Tainer, J. A. (1995) *J. Mol. Biol. 246*, 21−27.
35. Neuefeind, T., Huber, R., Reinemer, P., Knäblein, J., Prade, L., Mann, K., and Bieseler, B. (1997) *J. Mol. Biol. 274*, 577−587.
36. Neuefeind, T., Huber, R., Dasenbrock, H., Prade, L., and Bieseler, B. (1997) *J. Mol. Biol. 274*, 446−453.


BI980323W